Tiny Piezoelectric Harvesters: Principles, Constraints, and Power Conversion

Gabriel A. Rincón-Mora, *Fellow, IEEE*, and Siyu Yang, *Graduate Student Member, IEEE*

***Abstract*—Wireless microsystems can add intelligence to hospitals, homes, and factories that can save money, energy, and lives. Unfortunately, tiny batteries cannot store sufficient energy to sustain useful microsystems for long, and replacing or recharging the batteries of hundreds of networked nodes is costly and invasive in the case of the human body. Thankfully, shocks and vibrations are prevalent in many applications, so ambient kinetic energy can continually replenish batteries to extend the life of the systems they support. And since tiny devices produce minimal damping effects on motion, they can draw as much power as the microelectronics allow. Unfortunately, uncollected charge, breakdown voltages, and energy losses limit how much power harvesting microsystems can generate. This is why this paper reviews how tiny transducers generate power and how state-of-the-art diode bridges and switched inductors and their derivatives draw and output as much power as possible. Of prevailing technologies, in fact, the recycling bridge pre-damps the transducer at the highest voltage possible all the time to output the highest power. But because it still needs a regulating charger to stay at its maximum power point, other pre-damping switched inductors suffer lower losses and require less space. Although the pre-damping bridgeless solution pre-damps every other half cycle, it generates comparable power with only two switches. No harvester, however, escapes the limits that power losses and breakdown voltages impose, so output power is always finite, and in the case of miniaturized systems, not very high.**

***Index Terms*—Piezoelectric harvesters, ambient kinetic energy, motion, vibration, shock, diode bridges, switched inductors, harvesting chargers, and energy-harnessing microsystems.**

I. Harvesting Microsystems

Wireless microsystems that sense, monitor, manage, and report information in hospitals, homes, office buildings, factories, farms, and humans can save money, energy, and lives [1]. Although the power they require is nowadays low in the microwatt range [2], miniaturized batteries cannot store sufficient energy to sustain them for months or years at a time [3]. This is why drawing power from ambient sources is so popular today, because the environment is a vast tank that requires no board space.

Photovoltaic cells are popular in this respect because sunlight outputs the highest power levels at 10–15 mW/cm^2 [4]. The problem is solar light is often unavailable, and artificial lighting produces less than 100 μW/cm^2 [5]. Thankfully, shocks and vibrations are prevalent in automobiles, airplanes, machinery, and humans. Plus, electromechanical transducers can output moderate power. Of these, though, piezoelectric devices can produce more power at 300 μW/cm^3 than their electrostatic and electromagnetic counterparts can at 100 μW/cm^3 and 10 μW/cm^3 [6].

Still, micro-scale piezoelectric transducers harness a small fraction of ambient kinetic power, and only in the presence of shocks and vibrations. A system must therefore incorporate a rechargeable battery v_{BAT} that can supply power when ambient power is insufficient or unavailable [7]. The role of the transducer in Fig. 1, for example, is to recharge v_{BAT}. The aims of the piezoelectric harvester [8], feedback loop, and power supply are to draw power, keep the system at its maximum power point (MPP), and feed the power amplifier (PA), digital-signal processor (DSP), analog–digital converter (ADC), and the other functional blocks that comprise the load.

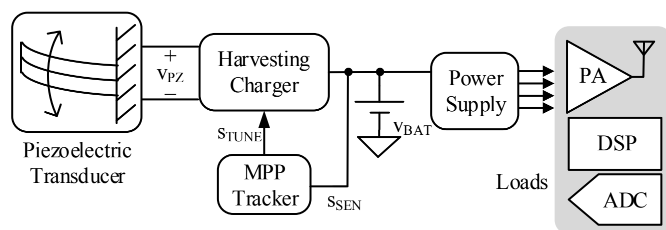

Fig. 1. Piezoelectric energy-harvesting microsystem.

This paper surveys, compares, and derives from the state of the art how tiny piezoelectric harvesters can generate power. Although not to the same extent, breadth, or depth, [8] and [40] similarly review some (but not all) the technologies and concepts presented here. In this rendition, Section II reviews how and under which conditions state-of-the-art micro-scale transducers output charge in the presence of motion. Sections III, IV, and V then describe and assess the latest in piezoelectric chargers and their derivatives. Sections VI and VII end with comparisons and conclusions.

II. Tiny Piezoelectric Transducers

A. Basic Operation

When unstrained, piezoelectric material is electrically neutral because, as Fig. 2a illustrates, positive and negative charge centers align and balance. The atomic arrangement is such, however, that charge centers shift away from one another when the material strains [9]. This shift produces a surface potential that changes continuously with variations in mechanical deformation.

A transducer must therefore incorporate a piece of piezoelectric material that strains in the presence of shocks

Manuscript received Month XX, 2015; revised Month XX, 2015; accepted Month XX, 2015.

The authors are with the School of Electrical and Computer Engineering at the Georgia Institute of Technology in Atlanta, Georgia 30332-0250 U.S.A. E-mail: Rincon-Mora@gatech.edu and jimsyyang@gatech.edu.

and vibrations. For this, only one end of the piezoelectric cantilever in Fig. 2b, for example, is stationary on a firm base and the other carries a mass [10]. This way, motion produces a displacement and strain that the mass extends. Once maximally strained, the cantilever springs back, and under favorable conditions, oscillates. The frequency at which the device will most easily oscillate depends on the tensile and elastic properties of the material and the size and weight of the mass. Although other mechanical configurations are possible, similar principles govern their design, operation, and properties.

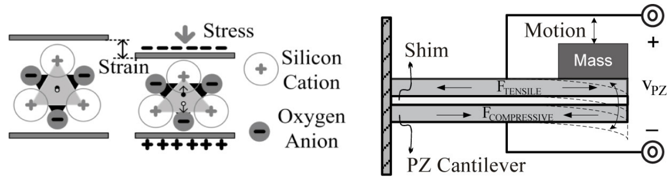

(a) (b)

Fig. 2. Piezoelectric (a) material and (b) transducer.

Table I lists the state of the art in tiny piezoelectric transducers [10], [12]–[15]. Unpackaged volumes range from 12 to 27 mm^3. They output 10–85 μW at 100–300 μW/cm^3, which is higher than what electrostatic transducers usually can [6], but as expected, lower than what sunlight can [4]. Natural frequencies range from 252 to 1300 Hz, which is slightly higher than the 1–300 Hz vibrations that most applications exhibit [11]. Unfortunately, [10], [12]–[15] did not quote capacitance, so how they compare with the nF's that commercially available transducers exhibit is not certain.

TABLE I. STATE-OF-THE-ART PIEZOELECTRIC TRANSDUCERS

Reference	Unpackaged Volume	Power	Frequency
[12]	12 mm^3	10 μW	252 Hz
[10]	19 mm^3	35 μW	572 Hz
[13]	0.021* mm^3	45 μW	1300 Hz
[14]	27 mm^3	68 μW	419 Hz
[15]	Not Reported	85 μW	325 Hz

*Volume of the active piezoelectric material (not the transducer).

B. Electrical Model

When motion pushes the cantilever away from its resting place, the material acquires a potential energy E_{PE} that climbs with displacement d_S and peaks when maximally displaced. The spring then pushes the mass M_S back with such force that velocity v_S and kinetic energy E_{KE} peak when d_S is back at zero. So mass swings in the other direction to repeat the process. The system continually exchanges potential and kinetic energies this way until impeding forces damp oscillations.

Like a spring, an inductor L_M can receive or release energy, but not hold it. So with a capacitor C_M in parallel, L_M's energy E_L first drains to C_M and C_M's energy E_C then depletes back into E_L and alternate this way until parasitic resistances R_M burn the energy. Since E_L and E_C rise with L_M's current i_{LM} and C_M's voltage v_{CM} like E_{PE} and E_{KE} with displacement d_S and velocity v_S, i_{LM} and v_{CM} in Fig. 3 can mimic d_S and v_S when L_M maps to the cantilever's spring constant K_S, C_M to M_S, and R_M to mechanical damping forces:

$$E_{PE} = 0.5K_S d_S^{\ 2} \equiv E_L = 0.5L_M i_{LM}^{\ 2} \tag{1}$$

$$E_{KE} = 0.5M_S v_S^{\ 2} \equiv E_C = 0.5C_M v_{CM}^{\ 2}\ . \tag{2}$$

A Norton-equivalent current source i_S can therefore emulate the shocks and vibrations that power the transducer. Thevenin-equivalent models, which use voltage sources and series components, can also model this behavior [16].

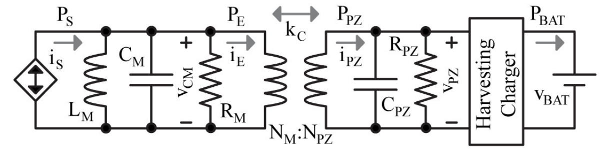

Fig. 3. Electrical model of a piezoelectric transducer.

The purpose of the transducer is to map mechanical energy into the electrical domain. In this case, M_S's kinetic energy in C_M corresponds to electrostatic energy in the cantilever's capacitance C_{PZ}. But since velocity v_{CM} does not equate to C_{PZ} voltage, the transformer turns ratio N_{PZ}/N_M maps v_{CM} to v_{PZ}:

$$\frac{N_{PZ}}{N_M} \equiv \frac{v_{PZ}}{v_{CM}}\ . \tag{3}$$

R_{PZ} then models the power that C_{PZ} leaks.

Power derived from the transducer is a power drain that damps oscillations. Of the power drawn with P_E in the mechanical domain, however, only a fraction couples to the electrical domain with P_{PZ}. This is why the power-converting transformer in Fig. 3 delivers an electromechanical fraction k_C^2 of what P_E supplies to P_{PZ} and keeps the rest in the mechanical domain. So P_E's equivalent resistance R_E in Fig. 4 effectively burns $1/k_C^2$ more power than P_{PZ}'s equivalent load R_L or v_{PZ}/i_{PZ}:

$$R_E = \frac{v_{CM}^{\ 2}}{P_E} \equiv \left(\frac{k_C^{\ 2}}{P_{PZ}}\right) v_{CM}^{\ 2} = k_C^{\ 2}\left(\frac{R_L}{v_{PZ}^{\ 2}}\right) v_{CM}^{\ 2} = R_L\left(\frac{N_M}{N_{PZ}}\right)^2 k_C^{\ 2}\ . \tag{4}$$

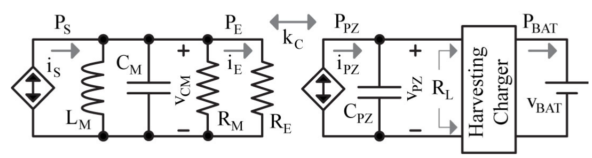

Fig. 4. Simplified under-damped model of a tiny piezoelectric transducer.

The small active piezoelectric area of tiny transducers output so little power that the electrical damping force imposed by P_E on the mechanical device is nearly always much lower than the counterpart that friction, air, and other mechanical forces pose with R_M's P_M. Being this under-damped [17] means P_E has negligible impact on velocity and displacement [18]. In other words, the transducer is effectively an independent Thevenin- or Norton-equivalent voltage or current source i_{PZ}, like in the case of Fig. 4. Thankfully, leakage is normally so low that R_{PZ} is negligible.

C. Maximum Power

When vibration frequency matches the resonant frequency of the tank, motion feeds energy that L_M and C_M exchange to produce an oscillating voltage that is in phase with i_S. As a result, i_S delivers power P_S across both positive and negative half cycles. The energy in the tank therefore grows as long as P_S surpasses R_M and R_E's combined losses. When losses match P_S, L_M and C_M supply each other's needs and R_M and R_E consume P_S. In other words, L_M and C_M in Fig. 4, for all practical purposes, disappear and R_M and R_E receive all of P_S.

When vibration and resonant frequencies do not match, however, v_M is no longer in phase with i_S. Although i_S still produces power when i_S and v_M are both positive and both negative, i_S now consumes power when their polarities oppose. The transducer therefore draws the greatest power from motion when tuned to vibrations.

Since additional P_E has little effect on the velocity and displacement of tiny under-damped devices, the fundamental aim of a harvester should be to draw the highest power possible. For this, the circuit should keep v_{PZ} in phase with i_{PZ} and at the highest level that the breakdown voltage allows. Except, conduction losses climb with drawn power, so when still below the breakdown level, v_{PZ} should rise until incremental losses cancel additional gains. In other words, frequency, breakdown voltage, and losses limit output power.

III. Basic Diode Bridges

The basic diode bridge in Fig. 5 is popular in this space because the diodes rectify and steer i_{PZ} into a receiving capacitor C_{REC} [19]. When assuming diode voltages are zero, for example, i_{PZ}'s positive half cycle in Fig. 6 charges C_{PZ} until v_{PZ} overcomes C_{REC}'s rectified output voltage v_{REC}. Past that point and through the end of the positive half cycle, diodes D_{PG} and D_{PO} steer i_{PZ} into C_{REC}. Similarly, i_{PZ} across negative half cycles discharges C_{PZ} until D_{NG} and D_{NO} clamp v_{PZ} to $-v_{REC}$, past which point i_{PZ} flows, again, into C_{REC}.

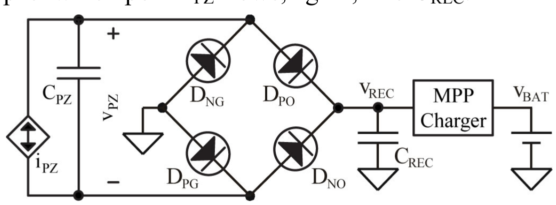

Fig. 5. Diode-bridge charger.

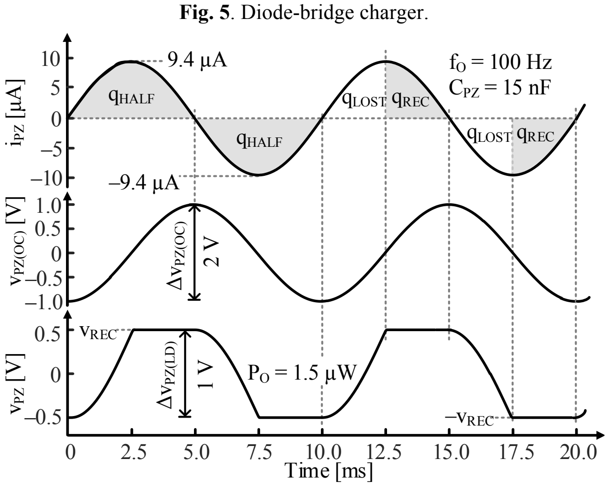

Fig. 6. Ideal diode-bridge waveforms.

Interestingly, raising v_{REC} increases the power i_{PZ} delivers into C_{REC} at v_{REC} as well as the charge lost to C_{PZ} when swinging v_{PZ} between v_{REC} and $-v_{REC}$. So for maximum power, the system should raise v_{REC} until the incremental loss cancels the additional gain, which happens at a particular v_{REC}. This is why a charger in Fig. 5 draws just enough power from C_{REC} to keep v_{REC} near its maximum power point.

To quantify this point, consider that, without the bridge, i_{PZ}'s half-cycle charge q_{HALF} in Fig. 6 would charge C_{PZ} across peak–peak open-circuit voltage $\Delta v_{PZ(OC)}$, so

$$q_{HALF} = C_{PZ}\Delta v_{PZ(OC)} . \tag{5}$$

But since C_{PZ} absorbs some of q_{HALF} when charging across $2v_{REC}$, C_{REC} loses charge q_{LOST} to C_{PZ}:

$$q_{LOST} = C_{PZ}\left(2v_{REC}\right) . \tag{6}$$

C_{REC} therefore collects with q_{REC} the difference every half cycle to harness with E_H twice q_{REC}'s energy per cycle:

$$E_H = 2\left(q_{HALF} - q_{LOST}\right)v_{REC} = 2C_{PZ}\left(\Delta v_{PZ(OC)}v_{REC} - 2v_{REC}^{\ 2}\right) . \tag{7}$$

The maximum power point results when the incremental loss in q_{LOST} balances the additional gain in q_{HALF}, which happens when the combined derivative is zero and v_{REC} is $0.25\Delta v_{PZ(OC)}$:

$$\frac{dE_H}{dv_{REC}} = 2C_{PZ}\left(\Delta v_{PZ(OC)} - 4v_{REC}\right)\Big|_{\Delta v_{PZ(LD)}=2v_{REC}=0.5\Delta v_{PZ(OC)}} \equiv 0 . \tag{8}$$

In other words, E_H peaks to $0.25C_{PZ}\Delta v_{PZ(OC)}^{\ 2}$ when the loaded swing $\Delta v_{PZ(LD)}$ is half the open-circuit counterpart $\Delta v_{PZ(OC)}$:

$$E_{H(MAX)} = 0.25C_{PZ}\Delta v_{PZ(OC)}^{\ 2} . \tag{9}$$

Output power P_O can therefore be $0.25C_{PZ}\Delta v_{PZ(OC)}^{\ 2}f_O$.

A. Cross-Coupled Bridge

Unfortunately, actual diodes drop 0.6–0.8 V when they conduct i_{PZ}, so they burn substantial power. Luckily, v_{REC} is sometimes greater than an NMOS threshold voltage v_{TN}. As a result, v_{PZ} rises high enough to close the cross-coupled NFETs in Fig. 7. Or viewed differently, v_{PZ} falls low enough below v_{REC} to close a cross-coupled PFET pair [20] in place of D_{PO} and D_{NO} in Fig. 5. This way, M_{NG} and M_{PG} drop less than 100 mV to reduce conduction losses by more than 83%.

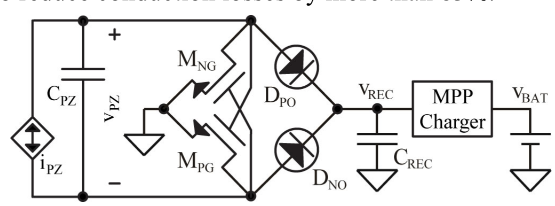

Fig. 7. Cross-coupled diode-bridge charger.

Notice M_{NG} and M_{PG} close whenever v_{PZ} rises above v_{TN}, which happens before v_{PZ} reaches v_{REC}. This is acceptable because D_{PO} and D_{NO} block i_{PZ} until v_{PZ} reaches v_{REC}. This is why PFETs cannot replace D_{PO} and D_{NO} when NFETs already replace D_{NG} and D_{PG}, because PFETs would also engage early. Shorting C_{PZ} to C_{REC} this way when v_{PZ} is below v_{REC} would drain C_{REC} into C_{PZ}. Replacing D_{PO} and D_{NO} with cross-coupled PFETs and inserting one diode D_{REC} between them and C_{REC}, however, like Fig. 8 [21] shows, works because D_{REC} blocks i_{PZ}. The tradeoff for reducing two diodes to one is adding one series resistance to the conduction path.

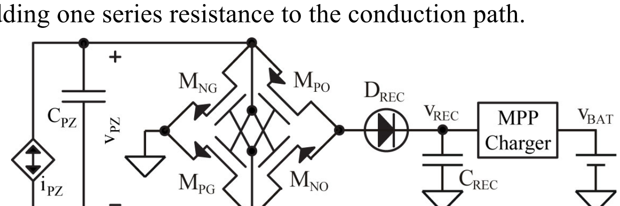

Fig. 8. Cross-coupled diode-bridge charger (negative voltage converter NVC).

B. Half Bridge

The half bridge in Fig. 9 also rectifies and steers i_{PZ} into C_{REC} [22]–[23]. Similar to the ideal full bridge, i_{PZ}'s positive half-cycle charge in Fig. 10 charges C_{PZ} until v_{PZ} overcomes v_{REC}, past which point D_{REC} conducts i_{PZ} into C_{REC}. i_{PZ}'s negative half-cycle charge then drains C_{PZ} until D_G clamps v_{PZ} to 0 V and steers the rest of i_{PZ}'s negative half-cycle charge to ground. This means, C_{REC} only harnesses positive charge.

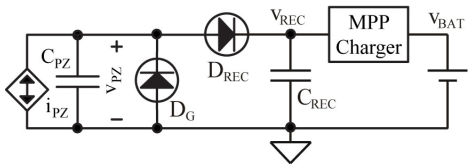

Fig. 9. Half-bridge charger.

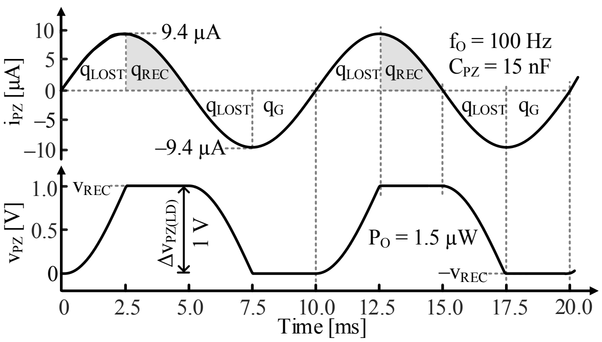

Fig. 10. Ideal half-bridge waveforms.

Ultimately, C_{REC} collects the positive charge that i_{PZ} does not lose to C_{PZ} when swinging v_{PZ} across v_{REC}. But like before, i_{PZ} delivers more power to C_{REC} with a higher v_{REC} and C_{PZ} loses more charge when swinging across a wider v_{REC}. So maximum power results at the v_{REC} that balances this tradeoff. This is why Fig. 9 includes a charger, to draw just enough power from C_{REC} to keep v_{REC} near its maximum power point.

To derive this maximum power point, first recall that i_{PZ}'s positive charge q_{HALF} is still $C_{PZ}\Delta v_{PZ(OC)}$. But since i_{PZ} loses positive charge q_{LOST} to C_{PZ} when charging to v_{REC}:

$$q_{LOST} = C_{PZ} v_{REC}\,, \tag{10}$$

C_{REC} collects with q_{REC} and E_H the difference at

$$E_H = \left(q_{HALF} - q_{LOST}\right) v_{REC} = C_{PZ}\left(\Delta v_{PZ(OC)} v_{REC} - {v_{REC}}^2\right). \tag{11}$$

Maximum power results when the incremental loss cancels the additional gain, or when the combined derivative is zero and v_{REC} is twice that of the full bridge at $0.5\Delta v_{PZ(OC)}$:

$$\frac{dE_H}{dv_{REC}} = 2C_{PZ}\left(\Delta v_{PZ(OC)} - 2v_{REC}\right)\Big|_{\Delta v_{PZ(LD)} = v_{REC} = 0.5\Delta v_{PZ(OC)}} \equiv 0\,. \tag{12}$$

In other words, C_{REC} collects half the charge of the full bridge at twice the voltage, so E_H can be the same: $0.25C_{PZ}\Delta v_{PZ(OC)}{}^2$. Plus, the optimum loaded swing $\Delta v_{PZ(LD)}$ is still $0.5\Delta v_{PZ(OC)}$.

C. Diode Options

As already mentioned, diodes can burn substantial conduction power when they steer i_{PZ} because they drop 0.6–0.8 V. Although replacing two diodes in the full bridge with cross-coupled FETs is possible when v_{REC} is greater than a MOS threshold voltage, the same is not true for all diodes in the full bridge or diodes in the half bridge. And if v_{REC} is less than 0.6–0.8 V, like in Fig. 6, replacing two diodes is not even possible.

Ideally, a diode should drop 0 V, lose 0 A, and respond instantly. Although on-chip Schottky and P–N junction diodes drop 0.4–0.6 V and 0.6–0.8 V, they lose no ground current and respond almost instantly. Similarly, the diode-connected FET in Fig. 11b drops a gate–source voltage v_{GS} that can be 0.6–0.9 V, loses 0 A, and although not to the same extent, responds very quickly.

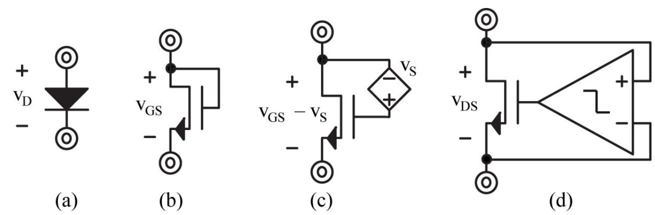

Fig. 11. Diode options.

The voltage source v_S in Fig. 11c shifts the FET's v_{GS} by v_S so the switch can drop $v_{GS} - v_S$, which can be 100–200 mV [24] and correspond to a 70%–90% reduction in conduction power. The voltage is not lower because the tolerance of MOS threshold voltages is high on the order of ±75–±100 mV [25], so margin must exist to ensure the FET does not conduct reverse current. Irrespective, the tradeoffs for this reduction in conduction power are quiescent power and response time, because v_S is a circuit that requires power and time to react.

The FET in Fig. 11d drops an even lower voltage because the comparator can overdrive the FET into triode when terminal voltages are only millivolts apart [26]. This way, the drain–source voltage v_{DS} can be 25–100 mV and the corresponding conduction loss 80%–97% lower than a diode. Like before, though, the tradeoffs are quiescent power and response time. But since conduction losses and tolerance are lower, this option is often preferable over the shifted counterpart.

Adding an input offset to the comparator so it transitions early can offset the delay of the circuit to reduce its effective response time [27]. Too much offset, however, can trip the comparator before it should. A more important consideration is how saved conduction power stacks against quiescent power and the power lost because of the comparator's delay. In other words, if saved power does not outweigh losses, which can be the case when i_{PZ} is low, a diode can be a lower-loss option.

IV. Basic Switched Inductors

A. Energy Transfers

The fundamental aim of inductors in energy harvesters is to transfer energy. When connected across a battery v_{BAT}, for example, an inductor L_X draws current and energy from v_{BAT}. In this case, L_X's energizing voltage v_E is v_{BAT}, and since v_{BAT} is fairly constant, L_X's current i_L rises linearly with time at the rate of v_E/L_X like Fig. 12a shows. So when L_X collects with i_L the desired amount of energy $0.5L_X i_{L(PK)}{}^2$ from v_{BAT} across energizing time t_E, the system disconnects L_X from v_{BAT}.

Draining L_X into a battery is similar, but in reverse. Here, once L_X has energy in the form of i_L, the system connects v_{BAT} across L_X such that L_X's voltage is negative. With such a de-energizing voltage v_D, i_L falls linearly with time to drain into

v_{BAT} at the rate of v_D/L_X. When L_X depletes, which happens when i_L is zero, the system disconnects L_X from v_{BAT}.

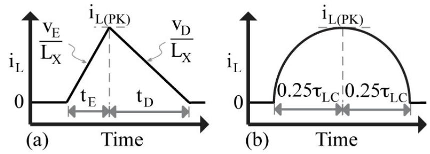

Fig. 12. Energy transfers with (a) batteries and (b) capacitors.

Drawing and supplying energy to a capacitor C_X is basically the same. When connecting an empty L_X across a charged C_X, for example, C_X discharges into L_X. But since C_X's voltage falls as C_X drains, i_L's rising rate decreases with time to produce the quarter sinusoid shown in Fig. 12b. Irrespective of C_X's initial energy, C_X drains completely into L_X after a quarter resonance period $0.25\tau_{LC}$. Supplying a capacitor is the same, but in reverse. When connecting an energized L_X across an empty C_X, L_X's i_L charges C_X, i_L drops more quickly as C_X's voltage rises, and L_X fully depletes after $0.25\tau_{LC}$.

Since peak currents $i_{L(PK)}$, inductances L_X, and piezoelectric capacitances C_{PZ} in small commercially available transducers are usually below 100 mA, 300 μH, and 50 nF and battery voltages v_{BAT} are above 1 V [27], transfers complete within 4 μs. So of the 3 ms to 1 s that a typical cycle can last [11], each transfer normally requires less than 0.2% of the vibration period. This means, transfers are practically instantaneous.

To carry energy without consuming much power, inductor currents and resistances should be low. For low currents, inductances should be high, and for low resistances, coils should be large. This is why many implementations use 100-μH to 10-mH inductors that occupy more than $6 \times 6 \times 3$ mm^3.

B. Synchronized Switched-Inductor Discharges

Basic switched-inductor harvesters use an inductor L_X to drain between cycles the charge that C_{PZ} collects across half cycles [29]. This way, with synchronous electric charge extraction (SECE), i_{PZ}'s positive half-cycle charge in Fig. 6 charges the unloaded C_{PZ} to $\Delta v_{PZ(OC)}$ in Fig. 13. At the end of i_{PZ}'s positive half cycle, L_X drains C_{PZ} into the battery v_{BAT}. i_{PZ}'s negative half-cycle charge then charges C_{PZ} to $-\Delta v_{PZ(OC)}$ and L_X drains C_{PZ} into v_{BAT} at the end of the half cycle.

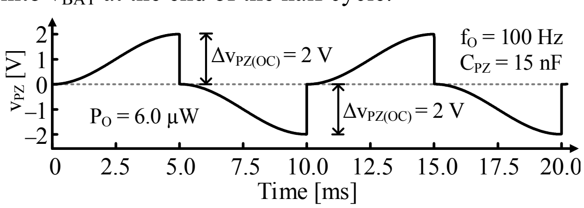

Fig. 13. Synchronized switched-inductor discharges.

Since v_{BAT} receives between half cycles the energy C_{PZ} collects across half cycles, v_{BAT} in one cycle harnesses with E_H twice the energy C_{PZ} collects with $\Delta v_{PZ(OC)}$:

$$E_H = E_{C(+)} + E_{C(-)} = 2\left(0.5C_{PZ}\Delta v_{PZ(OC)}{}^2\right) = C_{PZ}\Delta v_{PZ(OC)}{}^2. \quad (13)$$

Note this energy is 4× higher than that of basic diode bridges. One reason for this is basic bridges lose i_{PZ} charge to C_{PZ} when swinging v_{PZ} between rectified limits. Another reason is C_{PZ}'s energy rises quadratically with v_{PZ}, so the switched inductor collects more energy with 4× the loaded swing at $2\Delta v_{PZ(OC)}$ than the basic diode bridge does with $0.5\Delta v_{PZ(OC)}$.

Although L_X's series resistance (i.e., quality factor) and other losses limit some of these gains, a fundamental drawback and challenge with switched inductors is synchronizing switching events. Basic diode bridges draw piezoelectric power automatically whenever v_{PZ} overcomes its rectified output v_{REC}. Switched inductors, on the other hand, must synchronize energy transfers to i_{PZ}'s half-cycle points. This means, switched inductors require a power-consuming controller that basic bridges do not. Still, nanowatts for the controller is usually not enough to trump the microwatts that switched inductors gain over basic bridges [21], [30]–[33].

C. Bridged Switched Inductor

One way to synchronize discharges into v_{BAT} is to rectify v_{PZ} across half cycles with a bridge and drain C_{PZ} into v_{BAT} between half cycles with L_X like Fig. 14 shows [34]. This way, v_{REC} in Fig. 15 follows v_{PZ} across i_{PZ}'s positive half cycles to peak at $\Delta v_{PZ(OC)}$. When half cycles end, switch S_G closes long enough to drain C_{PZ} into L_X. When S_G opens, S_O closes and D_G conducts to deplete L_X into v_{BAT}. v_{REC} then mirrors v_{PZ} across i_{PZ}'s negative half cycles to peak at $\Delta v_{PZ(OC)}$, at which points S_G, D_G, and S_O drain C_{PZ} into L_X and L_X into v_{BAT}.

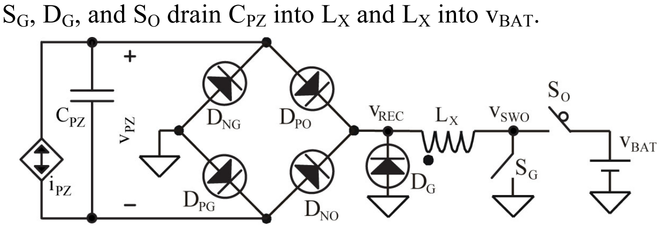

Fig. 14. Bridged switched inductor.

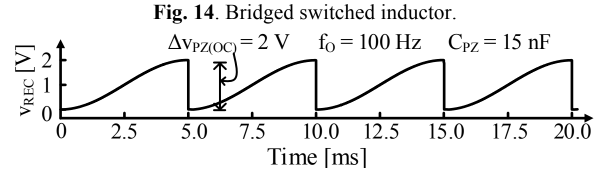

Fig. 15. Rectified piezoelectric voltage in the bridged switched inductor.

To reduce conduction losses, cross-coupled NFETs can replace D_{NG} and D_{PG} when $\Delta v_{PZ(OC)}$ is greater than an NMOS threshold voltage. Plus, since no component loads v_{REC} across half cycles, cross-coupled PFETs can also replace D_{PO} and D_{NO} when $\Delta v_{PZ(OC)}$ is greater than a PMOS threshold voltage [35]. If $\Delta v_{PZ(OC)}$ is high enough, C_{PZ} can drain into L_X and v_{BAT} with S_{REC} in Fig. 16 and L_X can then deplete into v_{BAT} with D_G [36]. The tradeoff for fewer switches is that $\Delta v_{PZ(OC)}$ must exceed v_{BAT} for the circuit to work.

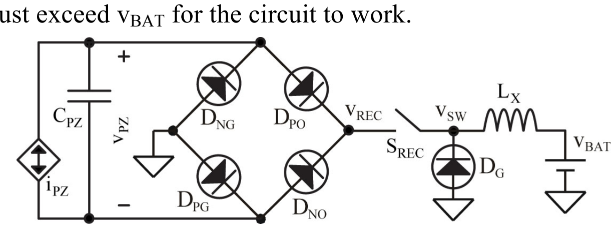

Fig. 16. Modified bridged switched inductor.

D. Bridgeless Switched Inductor

L_X in Fig. 17 discharges C_{PZ} directly without a bridge [37]. Here, i_{PZ} charges C_{PZ} across half cycles like Fig. 13 shows. At v_{PZ}'s positive peak $\Delta v_{PZ(OC)}$, S_N and S_P close long enough to drain C_{PZ} into L_X. Then, S_P opens and L_X's i_L flows through D_P

into v_{BAT} until L_X depletes. At the end of the negative half cycle, when v_{PZ} peaks at $-\Delta v_{PZ(OC)}$, S_N and S_P again close to drain C_{PZ} into L_X. Then, S_N opens and L_X's i_L, which is now flowing up toward v_{SW-}, flows through D_N into v_{BAT}.

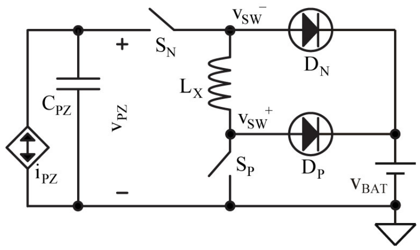

Fig. 17. Bridgeless switched inductor.

Fixing C_{PZ}'s bottom terminal to ground creates one subtle, though not insignificant disadvantage. The drawback is, C_{PZ}'s negative half-cycle voltage exposes S_N to negative voltages. This means, conventional CMOS switches must bias their P-type substrates to a voltage that is at least just as negative to isolate the switches from other devices in the die.

The circuit also suffers from one limitation worth noting. For D_N not to conduct when C_{PZ} drains into L_X at the end of i_{PZ}'s positive half cycle, v_{PZ}'s peak $\Delta v_{PZ(OC)}$ should not exceed v_{BAT}. This is usually not a problem for tiny transducers because they typically capture a very small fraction of the mechanical energy available.

V. Pre-Damping Switched Inductors

A. Pre-Damping

Fortunately, the power i_{PZ} produces climbs with v_{PZ}. As a result, pre-charging C_{PZ} between half cycles and allowing i_{PZ} to charge C_{PZ} above that level across half cycles, like Fig. 18 illustrates, draws more power from motion than without pre-charging C_{PZ} [38]. In other words, the system recovers much more than just the energy invested E_P to pre-damp C_{PZ} to v_P.

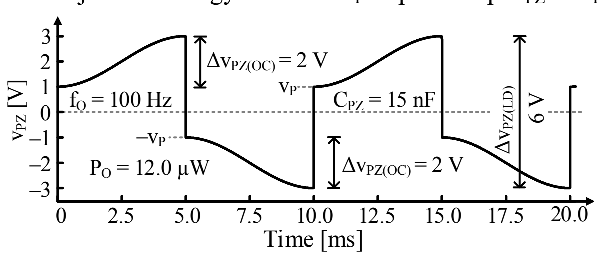

Fig. 18. Synchronized and pre-damped discharges.

To pre-damp C_{PZ} to v_P between half cycles, the system must first deposit E_P or $0.5C_{PZ}v_P^2$ into C_{PZ}. But since i_{PZ} charges C_{PZ} another $\Delta v_{PZ(OC)}$ across each half cycle, the system recovers $E_{C(PK)}$ or $0.5C_{PZ}(v_P + \Delta v_{PZ(OC)})^2$. So across an entire cycle, v_{BAT} invests and recovers twice these amounts to net E_H:

$$
\begin{aligned}
E_H &= 2\left(E_{C(PK)} - E_P\right) \\
&= 2\left[0.5C_{PZ}\left(v_P + \Delta v_{PZ(OC)}\right)^2 - 0.5C_{PZ}v_P^{\,2}\right]. \qquad (14) \\
&= C_{PZ}\Delta v_{PZ(OC)}^{\ \ 2} + 2C_{PZ}\Delta v_{PZ(OC)}v_P
\end{aligned}
$$

Not surprisingly, E_H here exceeds that of basic switched inductors. Plus, E_H grows with v_P, so v_P should be as high as breakdown voltage V_{BD} and power losses allow. This means, $v_P + \Delta v_{PZ(OC)}$ should not surpass V_{BD}, which is equivalent to saying v_P should remain below $V_{BD} - \Delta v_{PZ(OC)}$.

B. Bridged Switched Inductors

L_{P+} and L_{P-} in the bridged switched inductor of Fig. 19 pre-damp C_{PZ} to v_P between half cycles, like just described, to increase the voltage with which i_{PZ} sources power. [39] does pretty much the same, but with more switches. In all, the bridge rectifies v_{PZ} across half cycles so L_X can drain C_{PZ} into v_{BAT} and L_{P+} and L_{P-} can pre-damp C_{PZ} between half cycles. So just before a positive half cycle, S_+ closes to energize both L_{P+} and C_{PZ}. When v_{PZ} surpasses v_{BAT}, L_{P+} begins to drain into C_{PZ} what L_{P+} collected before v_{PZ} reached v_{BAT}. The controller then opens S_+ when L_{P+} depletes, at which point v_{PZ} is at v_P.

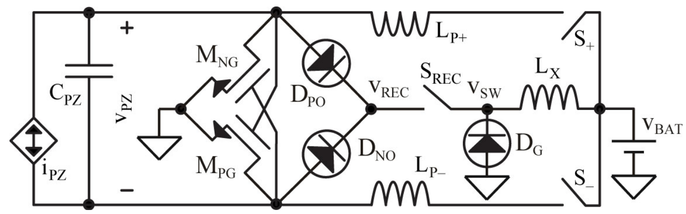

Fig. 19. Bridged switched inductors.

When the positive half cycle ends, when v_{PZ} peaks to $v_P + \Delta v_{PZ(OC)}$, S_{REC} closes to drain C_{PZ} into L_X and v_{BAT}, and when v_{PZ} falls below v_{BAT}, C_{PZ} and L_X deplete into v_{BAT}. If L_X still has energy when v_{PZ} is zero, S_{REC} opens and D_G steers what remains in L_X into v_{BAT}. Also at this point, S_- and L_{P-} mirror the action of S_+ and L_{P+} to pre-charge C_{PZ} to $-v_P$. S_- therefore closes to energize L_{P-} and C_{PZ} in the negative direction, L_{P-} begins to drain into C_{PZ} when $-v_{PZ}$ surpasses v_{BAT}, and when L_{P-} depletes, S_{N-} opens.

Notice M_{PG} and M_{NG} steer current into ground when S_+ and S_- pre-damp C_{PZ}. This means, diodes cannot replace M_{PG} and M_{NG}. Cross-coupled PFETs, however, can replace D_{PO} and D_{NO} because S_{REC} keeps the FETs from conducting when v_{PZ} engages them (before reaching $\Delta v_{PZ(OC)}$). But since D_{PO} and D_{NO} are in series with S_{REC}, switches in place of D_{PO} and D_{NO} can incorporate the functionality of S_{REC}. In other words, removing S_{REC} and replacing D_{PO} and D_{NO} with switches that a controller commands is possible. This way, their combined series resistance and losses are lower.

This system suffers from one subtle limitation. For L_{P+} and L_{P-} to drain, their voltages must reverse polarity, which can only happen if v_P surpasses v_{BAT}. In other words, this circuit works when the optimal pre-damping voltage is higher than v_{BAT}. This, however, is not a significant limitation when the transducer is under-damped, the breakdown voltage is higher than v_{BAT}, and incremental losses when v_P is above v_{BAT} do not cancel additional gains.

C. Recycling and Bridged Switched Inductors

The switched inductors and bridge in Fig. 20 similarly pre-damp C_{PZ} after synchronized discharges [40]. Here, the bridge rectifies across half cycles, L_X drains C_{PZ} partially into v_{BAT}, and L_R recycles what is left in C_{PZ} back into C_{PZ} to pre-damp C_{PZ} in the opposite direction. So when v_{PZ} peaks at $v_P + \Delta v_{PZ(OC)}$, S_{REC}, D_G, and L_X drain C_{PZ} partially to v_P. S_R then depletes C_{PZ} into L_R, and with S_R still closed, L_R returns C_{PZ}'s energy to pre-damp C_{PZ} to $-v_P$. At the next half cycle, S_{REC},

D_G, and L_X similarly drain C_{PZ} from $-(v_P + \Delta v_{PZ(OC)})$ to $-v_P$ and S_R and L_R recycle what is left to pre-charge C_{PZ} to v_P.

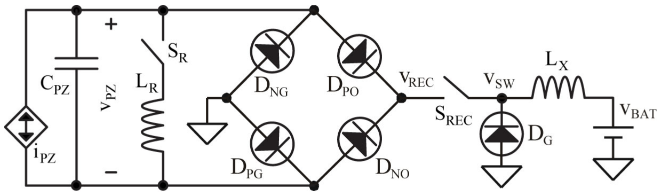

Fig. 20. Recycling and bridged switched inductors.

To follow the flow of energy into v_{BAT} more closely, the bridge and S_{REC} first discharge C_{PZ} into L_X and v_{BAT} until v_{PZ} falls to v_P. S_{REC} then opens, so L_X's i_L flows from ground to v_{BAT} through D_G until L_X exhausts its energy into v_{BAT}. The same happens at the end of the negative half cycle: S_{REC} discharges C_{PZ} into L_X and v_{BAT} until v_{PZ} is $-v_P$ and D_G then depletes L_X into v_{BAT}. In other words, v_{BAT} receives part of the energy C_{PZ} collects across half cycles when S_{REC} closes and the rest when S_{REC} opens. And L_R recycles the energy required to pre-damp C_{PZ} to v_P and $-v_P$.

If $\Delta v_{PZ(OC)}$ exceeds the threshold voltages of N- and P-type MOSFETs, cross-coupled NFETs can replace D_{NG} and D_{PG} and cross-coupled PFETs can replace D_{PO} and D_{NO}. Since D_{PO} and D_{NO} are in series with S_{REC}, switches in place of D_{PO} and D_{NO} can incorporate the functionality of S_{REC}. Removing S_{REC} and replacing D_{PO} and D_{NO} with switches that a controller commands is therefore possible.

One limitation worth noting is $v_P + \Delta v_{PZ(OC)}$ must exceed v_{BAT} for C_{PZ} to drain into L_X and v_{BAT}. In other words, pre-damping must be high enough and vibrations strong enough to charge C_{PZ} to a level that is higher than v_{BAT}. Like before, this is not a problem when the transducer is under-damped, breakdown voltage is higher than v_{BAT}, and the incremental losses of a higher v_P do not cancel additional gains. Using S_G (and S_{REC}) in Fig. 21 [33] to deplete C_{PZ} into L_X and D_O (with D_G) to later drain L_X into v_{BAT} circumvents this limitation. The tradeoff for removing this limitation is more switches.

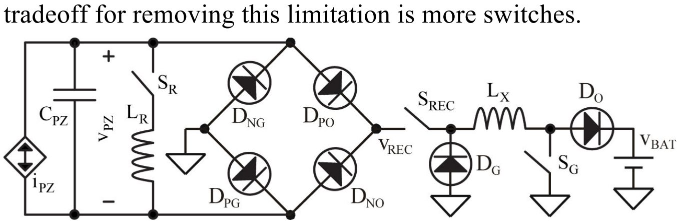

Fig. 21. Modified recycling and bridged switched inductors.

D. Switched-Inductor Bridge

Instead of relegating pre-damping and harvesting tasks to separate inductors, Fig. 22 reconciles those two functions into one [41]. So when v_{PZ} peaks, S_{PZ} closes to drain C_{PZ} into L_X and v_{BAT}. Then, when v_{PZ} falls below v_{BAT}, both C_{PZ} and L_X drain into v_{BAT}. And finally, when v_{PZ} reaches zero, leftover energy in L_X pre-damps C_{PZ} to a negative voltage, after which D_{PO} and S_{PZ} open. At the next half cycle, the sequence repeats, but in reverse: C_{PZ} drains into L_X and v_{BAT}, both C_{PZ} and L_X drain into v_{BAT}, and then leftover energy in L_X pre-damps C_{PZ}.

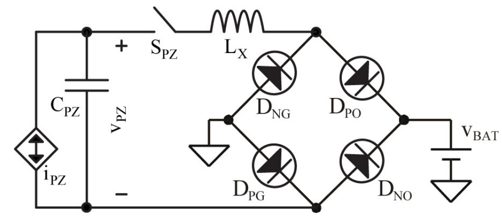

Fig. 22. Switched-inductor or series SSHI diode bridge.

Since L_X draws and drains the same energy with mirrored energizing and de-energizing voltages, L_X drains with ground and v_{BAT} what L_X draws with $2v_{BAT}$ at C_{PZ} and v_{BAT}. This means, C_{PZ} and L_X both exhaust at 0 V when $\Delta v_{PZ(OC)}$ is twice v_{BAT}. Without leftover energy in L_X, however, the system discharges, but does not pre-damp C_{PZ} between half cycles to behave like basic switched inductors, like Fig. 13 shows. So to pre-damp C_{PZ}, $\Delta v_{PZ(OC)}$ must exceed $2v_{BAT}$.

But with leftover energy used to pre-damp C_{PZ}, v_{PZ} surpasses $\Delta v_{PZ(OC)}$ in the next half cycle to produce even more leftover energy. Leftover energy therefore rises over time to produce the growing oscillations in Fig. 23. v_{PZ} stops swelling when the rise in drawn power in the mechanical domain balances mechanical damping forces, or when the rise in conduction losses cancels the rise in drawn power. In other words, output power climbs until the transducer is no longer under-damped or power losses outpace gains.

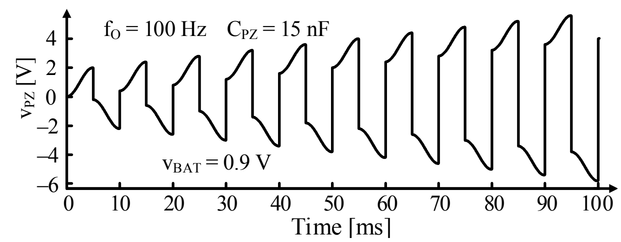

Fig. 23. Growing oscillations in a switched-inductor diode bridge.

Finding the maximum power point this way, automatically, is appealing when breakdown voltage and other power losses do not limit output power first. Unfortunately, over-damping a tiny transducer is very difficult. So if unchecked, either the circuit exceeds its breakdown limit or incremental power losses in the system outpace additional gains before conduction losses alone do. In other words, either the circuit breaks or outputs less power than possible.

When $\Delta v_{PZ(OC)}$ is less than $2v_{BAT}$, L_X depletes before C_{PZ}, so output diodes open and i_{PZ} finishes draining C_{PZ}. i_{PZ} therefore has less charge with which to energize C_{PZ}, so end-of-cycle energy is lower than in the previous cycle. With less initial energy, i_{PZ} loses more charge, so subsequent half cycles output less charge to produce the fading oscillations in Fig. 24.

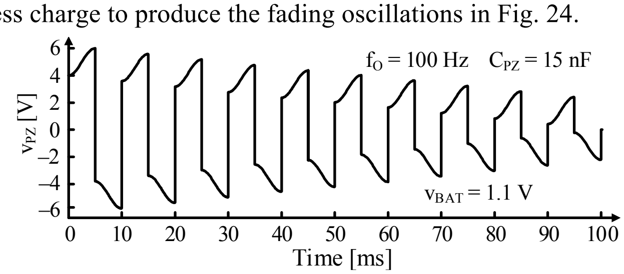

Fig. 24. Fading oscillations in a switched-inductor diode bridge.

Since D_{PO} and D_{NO} are in series with S_{PZ}, switches in place of D_{PO} and D_{NO} can incorporate the functionality of S_{PZ}. So removing S_{PZ} and replacing D_{PO} and D_{NO} with switches that a controller commands is possible. And if $\Delta v_{PZ(OC)}$ exceeds an NMOS threshold voltage, cross-coupled NFETs can also replace D_{NG} and D_{PG}.

Incorporating S_{PZ} into D_{PO} and D_{NO} in the guise of S_{PO} and S_{NO} and replacing D_{NG} and D_{PG} with the synchronous switches in Fig. 25 avails other switching configurations that can ensure lossless oscillations always grow [42]. The network can also limit how much energy drains into v_{BAT} when $\Delta v_{PZ(OC)}$ is less than $2v_{BAT}$ to ensure L_X has sufficient leftover energy to pre-damp C_{PZ} to v_P and $-v_P$ like Fig. 18 illustrates. For this, S_{PO} and S_{PG} can, like before, drain C_{PZ} into L_X and v_{BAT}. But unlike [42], S_{PO} opens when C_{PZ} and L_X hold enough energy to pre-damp C_{PZ}. So when S_{NG} closes, C_{PZ} depletes into L_X and L_X back into C_{PZ} to pre-charge C_{PZ} to $-v_P$. At the end of the negative half cycle, S_{NO} and S_{NG} similarly drain C_{PZ} into L_X and v_{BAT}, S_{NO} opens and S_{PG} closes to deplete C_{PZ} into L_X and L_X back into C_{PZ} to pre-damp C_{PZ} to v_P.

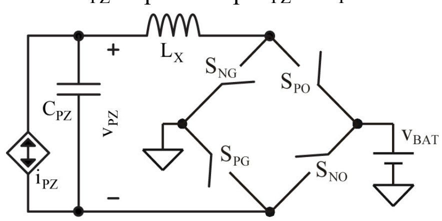

Fig. 25. Synchronous switched-inductor bridge.

E. *Bridgeless Switched Inductor*

Interestingly, the bridgeless switched inductor in Fig. 26 pre-damps only i_{PZ}'s negative half cycle [43]. This is acceptable when under-damped to the extent that drawn power has negligible effects on cantilever displacement and velocity. This may also be desirable in applications that call for asymmetrical damping of the moving cantilever.

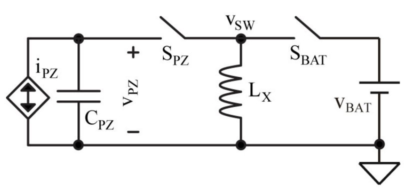

Fig. 26. Pre-damping bridgeless switched inductor.

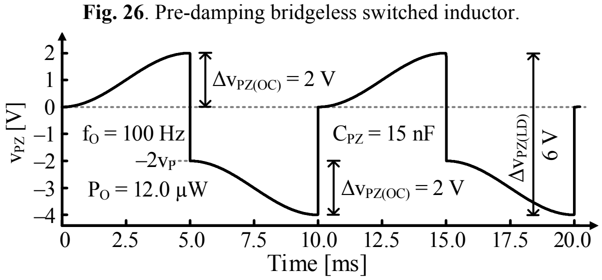

Fig. 27. Bridgeless switched-inductor voltage.

Operationally, i_{PZ} charges C_{PZ} across i_{PZ}'s positive half cycles to $\Delta v_{PZ(OC)}$. At that point, S_{BAT} closes to draw pre-damping energy from v_{BAT} into L_X. S_{BAT} then opens and S_{PZ} closes to deplete C_{PZ} into L_X. S_{PZ} remains closed long enough to cycle L_X's combined energy back to C_{PZ}. This way, C_{PZ} pre-damps to a level $-2v_P$ in Fig. 27 that v_{BAT}'s investment controls. i_{PZ} then charges C_{PZ} across i_{PZ}'s negative half cycle to $-(2v_P + \Delta v_{PZ(OC)})$. At that point, S_{PZ} first closes to deplete C_{PZ} into L_X. Once drained, when v_{PZ} is zero, S_{PZ} opens and S_{BAT} closes to drain L_X into v_{BAT}. This sequence then repeats.

As with its bridgeless predecessor from Fig. 17, C_{PZ}'s negative half-cycle voltage exposes S_{PZ} to negative voltages. Conventional CMOS switches must therefore bias their P-type substrates to a voltage that is at least just as negative to isolate the switches from other devices in the die. This is a subtle, though not insignificant requirement for this circuit.

F. *Recycling Switched-Inductor Bridge*

The switched-inductor in Fig. 28 adopts a different approach [44]. Here, L_R recycles the charge that i_{PZ} loses the first time i_{PZ} charges C_{PZ} across the bridge's $2v_{REC}$ so C_{REC} can receive all of i_{PZ}'s charge after that. For this, S_R closes between half cycles to drain C_{PZ} into L_R and L_R back into C_{PZ} and swing v_{PZ} in Fig. 29 from v_{REC} to $-v_{REC}$ at the end of the positive half cycle and back from $-v_{REC}$ to v_{REC} at the end of the other half. Since v_{PZ} is already at v_{REC} before new half cycles begin, all of i_{PZ}'s charge flows into C_{REC}.

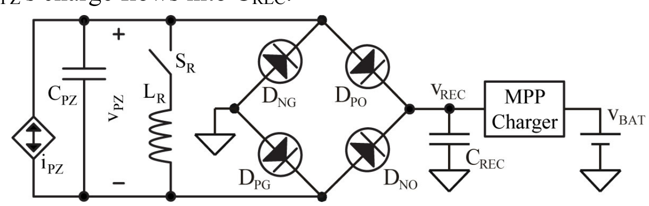

Fig. 28. Recycling switched-inductor or parallel SSHI diode bridge.

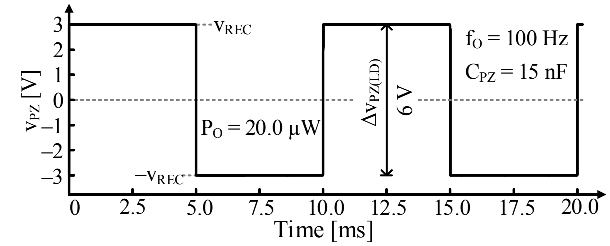

Fig. 29. Recycled switched-inductor diode-bridge voltage waveform.

This strategy features two important traits. First, C_{REC} collects all i_{PZ}'s charge. Second, since i_{PZ} no longer loses charge to C_{PZ}, v_{PZ}'s loaded swing $\Delta v_{PZ(LD)}$ need no longer halve v_{PZ}'s unloaded counterpart $\Delta v_{PZ(OC)}$. As a result, no tradeoff counters the rise in power that i_{PZ} produces at v_{REC} when v_{REC} is higher. C_{REC} can therefore collect twice i_{PZ}'s half-cycle charge q_{HALF} at the highest possible v_{REC} all the time:

$$E_H = 2q_{HALF}v_{REC} = 2C_{PZ}\Delta v_{PZ(OC)}v_{REC} \le 2C_{PZ}\Delta v_{PZ(OC)}V_{BD}\,. \quad (15)$$

But since v_{BAT} is seldom at the breakdown voltage V_{BD}, the recycling diode bridge cannot charge v_{BAT} directly. So like its predecessor, the circuit requires a maximum power-point charger. The basic aim of the charger is, like before, to draw just enough power to keep v_{REC} near V_{BD}.

VI. COMPARISON

A. *Output Power*

Actual output power is often more the result of application and implementation than fundamental principles. Space and process technologies, for example, dictate inductor's resistance, switches' resistances and capacitances, and controller's operating power, almost none of which are uniform in literature. This is why comparing output power or conversion efficiencies of reported implementations can be misleading when starting a design. Comparing possibilities and guiding principles are more important in this respect.

Half bridges generate as much power as full bridges because, at their maximum power points, they collect half the charge at twice the voltage. Basic switched inductors, however, collect all the charge to output four times the energy that basic bridges can. But since under-damped piezoelectric transducers source more power with higher voltages, pre-damping switched inductors, which pre-charge C_{PZ} between half cycles, output even more power. In fact, the recycling switched-inductor bridge produces the highest power because C_{REC} collects i_{PZ}'s charge at the highest possible voltage all the time.

Pre-damping circuits, however, can only output as much power as their breakdown voltages allow. Still, under similar loaded-swing limits, the recycling bridge outputs more power. With ±9.4 µA, 15 nF, and a 6-V limit, for example, all other pre-damping switched inductors output 40% less power at 12 µW than the recycling bridge at 20 µW, as the lossless simulations in Figs. 17, 26, and 28 demonstrate.

Power losses, however, offset these gains to, in some cases, negate their benefits. Although controllers can nowadays consume microwatts or less [21], [30]–[33], switches in the power-conduction path can lose tens of microwatts or more to gate drive and ohmic power [43]. This is why bridgeless schemes can, with only two to four switches, out-power their in-class competitors. The recycling bridge, for example, like all other bridges, requires a charger that draws just enough power to keep its rectified output at its maximum power point. But since chargers typically rely on at least two switches to transfer power [46], seven switches can burn the additional power that the recycling bridge can produce. Plus, the synchronizing controller that switches the inductor and the buffer that regulates the intermediate rectified voltage require more quiescent power than either on its own, which means quiescent power for the recycling bridge is also higher.

These conclusions hinge on under-damped conditions to persist. If harvesting chargers over-damp transducers before they reach their breakdown limits, the power-producing benefits of pre-damping systems disappear. What matters then are power losses, which means the bridgeless two-switch configuration will probably output the highest power.

The challenge with the two-switch topology is v_{BAT} only collects energy after negative half cycles. This means, the system damps the transducer across negative half cycles more than across positive half cycles, so the cantilever bends less in that direction than in the other. This may not be a problem when heavily under-damped because damping effects on displacement can be negligible. But when nearing over-damped conditions, when the two-switch solution wins over competing technologies, asymmetrical damping may compromise the mechanical stability of the transducer.

Near over-damped conditions, the next least power-consuming system is the four-switch bridgeless sibling. This one, however, like its two-switch counterpart, requires a negative supply, which again, consumes power. But since the purpose of the negative supply is to bias the substrate, it does not transfer much power, so power losses can be low.

B. Integration

When considering microsystems, reducing the number of off-chip components is paramount. Although basic bridges do not require regulating chargers to output power, they cannot operate at their maximum power point without the chargers. Efficient chargers, however, use at least one off-chip inductor to transfer power [46]. So all harvesters in the state of the art ultimately require no less than one inductor, as Table II shows.

But since basic bridges and the recycling bridge also require a rectifying capacitor, basic switched inductors, the switched-inductor bridge, and the bridgeless pre-damping switched inductor require less board space (for just one inductor). Of these, with only two switches, the pre-damping bridgeless scheme occupies the least silicon area. For reference, [38] used a 2.7-cm cantilever that integrates 25.4 × 3.8 × 0.25 mm^3 of piezoelectric material and a 330-µH surface-mount inductor with 1.6 Ω of series resistance that occupies 6 × 6 × 3.5 mm^3.

VII. Conclusions

Of prevailing and derived technologies, the recycling bridge outputs the highest power because the transducer outputs charge that the system collects at the highest possible voltage all the time. The pre-damping bridgeless switched inductor is next, and with only one inductor and two switches, this bridgeless option occupies less board space and less silicon

TABLE II. COMPARISON OF THE STATE OF THE ART

	Basic Bridges		Basic Switched Inductors		Pre-Damping Switched Inductors				
	Full	**Half**	**Bridged SL**	**Bridgeless**	**Bridged SL's**	**Rec. Bridged SL**	**SL Bridge**	**Bridgeless**	**Rec. Bridge**
Collected Charge	1/2	1/4	All	All	All	All	All	All	All
Max. Energy/Cycle	$0.25C_{PZ}\Delta v_{PZ(OC)}^2$		$C_{PZ}\Delta v_{PZ(OC)}^2$		$C_{PZ}\Delta v_{PZ(OC)}^2 + 2C_{PZ}\Delta v_{PZ(OC)}v_P$				$2C_{PZ}\Delta v_{PZ(OC)}v_{REC}$
Damping	Sym.	Asym.	Sym.	Sym.	Sym.	Sym.	Sym.	Asym.	Sym.
Pre-Damping	–	–	–	–	$\pm v_P$	$\pm v_P$	$\pm v_P$	$-2v_P$	$\pm V_{BD}$
Switches	4+	2+	6	4	8	7	5	2	5+
Inductors	1	1	1	1	3	2	1	1	2
C_{REC}	1	1	–	–	–	–	–	–	1
Control	Charger	Charger	Sync.	Sync.	Sync.	Sync.	Sync.	Sync.	Sync. + Charger
Negative Supply	–	–	–	V_{SS}	–	–	–	V_{SS}	–
Limitations	–	–	[1]$v_{PZ} > v_{BAT}$	$v_{PZ} \leq v_{BAT}$	$v_P > v_{BAT}$	[2]$v_{PZ} > v_{BAT}$	$v_{PZ} < 2v_{BAT}$	–	–

*Buffer normally requires one inductor and additional switches. [1]Removing this limitation requires one switch. [2]Removing this limitation requires two switches.

area. Plus, when over-damped conditions limit drawn power, this two-switch solution consumes less power, so it outputs more power than the recycling diode bridge. But if asymmetrical damping compromises the mechanical stability of the transducer, the four- and five-switch bridgeless sibling and synchronous switched-inductor bridge are better options. Since under-damped conditions prevail in most micro-scale applications, however, the benefits of the recycling diode bridge and pre-damping bridgeless options are ultimately difficult to discount.

REFERENCES

[1] D. Puccinelli and M. Haenggi, "Wireless sensor networks: applications and challenges of ubiquitous sensing," *IEEE Circuits Syst. Mag.*, vol. 3, no. 3, pp. 19–29, 2005.

[2] M. Fojtik, D. Kim, G. Chen, Y. Lin, D. Fick, J. Park, M. Seok, M. Chen, Z. Foo, D. Blaauw, and D. Sylvester, "A Millimeter-Scale Energy-Autonomous Sensor System With Stacked Battery and Solar Cells," *IEEE J. Solid-State Circuits*, vol. 48, no. 3, pp. 801–813, Mar. 2013.

[3] S Sudevalayam and P. Kulkarni, "Energy harvesting Sensor Nodes: Survey and Implications," *IEEE Comm. Surveys Tutorials,* vol. 13, no. 3, 2011.

[4] R.D. Prabha and G.A. Rincón-Mora, "0.18-µm Light-Harvesting Battery-Assisted Charger–Supply CMOS System," *IEEE Trans. on Power Electronics* [Early Access].

[5] N.J. Guilar, T.J. Kleeburg, A. Chen, D.R. Yankelevich, and R. Amirtharajah, "Integrated solar energy harvesting and storage," *IEEE Trans. Very Large Scale Integr. (VLSI) Syst.*, vol. 17, no. 5, pp.627–637, May 2009.

[6] S.P. Beeby, M.J. Tudor, and N.M. White, "Energy Harvesting Vibration Sources for Microsystem Applications," *Meas. Sci. Technol.,* vol. 17, pp. R175–195, Dec. 2006.

[7] G. Zhou, L. Huang, W. Li, and Z. Zhu, "Harvesting Ambient Environmental Energy for Wireless Sensor Networks: A Survey," *J. Sensors*, pp. 815467–815486, 2014.

[8] G. Szarka and B. Stark, "Review of Power Conditioning for Kinetic Energy Harvesting Systems," *IEEE Trans. on Power Electronics*, vol. 27, no. 2, pp. 803–815, 2012.

[9] K.A. Cook-Chennault, N. Thambi, and A.M. Sastry, "Powering MEMS portable devices– a review of non-regenerative and regenerative power supply systems with special emphasis on piezoelectric harvesting systems," *Smart Mater. Struct.*, vol. 17, no. 4, p. 043001 (33 pp.), Aug. 2008.

[10] A.B. Dow, A. Bittner, U. Schmid, and N.P. Kherani, "Design, Fabrication and Testing of a Piezoelectric Energy Microgenerator," *Microsystem Technol.*, vol. 20, pp. 1035–1040, Apr. 2014.

[11] S. Roundy, P.K. Wright, and J. Rabaey, "A study of low level vibrations as a power source for wireless sensor nodes," *Computer Communication*, vol. 26, pp. 1131–1144, Jul. 2003.

[12] E.E. Aktakka, R. Peterson, and K. Najafi, "A CMOS-compatible piezoeelctric vibration energy scavenger based on the integration of bulk PZT films on silicon," *Proc. of 2010 IEEE International Electron Devices Meeting*, pp. 31.5.1–31.5.4, 2010.

[13] A. Hajati and S. Kim, "Ultra-wide bandwidth piezoelectric energy harvesting," *Appl. Phys. Letter*, vol. 99, no. 8, pp. 083105–083108, Aug. 2011.

[14] E.E. Aktakka, R. Peterson, and K. Najafi, "A self-supplied inertial piezoelectric energy harvester with power-management IC," *IEEE Int'l Solid-State Circuits Conf.*, pp. 120–121, 2011.

[15] R. Elfrink, V. Pop, D. Hohlfeld, T. M. Kamel, S. Matova, C. de Nooijer, M. Jambunathan, M. Goedbloed, L. Caballero M. Renaud, J. Penders, and R. van Schaijk, "First autonomous wireless sensor node powered by a vacuum-packaged piezoelectric MEMS energy harvester," *Proc. of 2009 IEEE International Electron Devices Meeting*, pp. 1–4, 2009.

[16] Y. Ramadass and A. Chandrakasan, "An Efficient Piezoelectric Energy Harvesting Interface Circuit Using a Bias-Flip Rectifier and Shared Inductor," *IEEE J. Solid-State Circuits,* vol. 45, no. 1, pp. 189–204, Jan. 2010.

[17] R.J.M. Vullers, R. van Schaijk, I. Doms, C. van Hoof, and R. Mertens, "Micropower energy harvesting," *Solid-State Electronics*, vol. 53, no. 7, pp. 684–693, Jul. 2009.

[18] M. Marzencki, Y. Ammar, and S. Basrour, "Integrated Power Harvesting System Including a MEMS Generator and a Power management Circuit," *Sensor Actuators A Physical,* vol. 146–146, no. 1-2, pp. 363-370, Jul./Aug. 2008.

[19] G. Ottman, H. Hofmann, A. Bhatt, and G. Lesieutre, "Adaptive Piezoelectric Energy harvesting Circuit for Wireless Remote Power Supply," *IEEE Trans. on Power Electronics*, vol. 17, no. 5, pp. 669–676, May. 2002.

[20] C. Lu, C.Y. Tsui, and W.H. Ki, "Vibration energy scavenging system with maximum power tracking for micropower applications," *IEEE Trans. Very Large Scale Integr. (VLSI) Syst* , vol. 19, no. 11, pp. 2109–2119, Nov. 2011.

[21] T. Hehn, F. Hagedorn, D. Maurath, D. Marinkovic, I. Kuehne, A. Frey, and Y. Manoli, "A Fully Autonomous Integrated Interface Circuit for Piezoelectric Harvesters," *IEEE J. Solid-State Circuits*, vol. 47, no. 9, Sep. 2012.

[22] A. Tabesh and l.C. Grechette, "A Low-Power Stand-Alone Adaptive Circuit for Harvesting Energy from a Piezoelectric Micropower Generator", *IEEE Trans. Industrial Electronics*, vol. 57, no. 3, pp. 840–849, Mar. 2010.

[23] T.T. Le, J. Han, A. Von Jouanne, K. Mayaram, and T.S. Fiez, "Piezoelectric micro-power generation interface circuits," *IEEE J. Solid-State Circuits*, vol. 41, no. 6, pp. 1411–1420, Jun. 2006.

[24] C. Peters, J. Handwerker, F. Henrici, M. Ortmanns, and Y. Manoli, "Experimental results on power efficient single-poly floating gate rectifiers," *IEEE Int. Symp. Circuits and Syst.*, pp. 1097–1100, May 2009.

[25] T. Umeda, H. Yoshida, S. Sekine, Y. Fujita, T. Suzuki, and S. Otaka, "A 950-MHz rectifier circuit for sensor network tags with 10-m distance," *IEEE J. Solid-State Circuits*, vol. 41, no. 1, pp. 35–41, Jan. 2006.

[26] S. Guo and H. Lee, "An efficiency-enhanced CMOS rectifier with unbalanced-biased comparators for transcutaneous-powered high-current implants," *IEEE J. Solid-State Circuits*, vol. 44, no. 6, pp. 1796–1804, June 2009.

[27] O. Lazaro and G.A. Rincón-Mora, "180-nm CMOS wideband capacitor-free inductively coupled power receiver and charger," *IEEE J. Solid-State Circuits*, vol. 48, no. 11, pp. 2839–2849, Nov. 2013.

[28] R.D. Prabha, D. Kwon, O. Lazaro, K.D. Peterson, and G.A. Rincón-Mora, "Increase Electrical Damping in Energy-Harnessing Transducers," *IEEE Trans. on Circuits and Syst. II, Exp. Briefs*, vol. 58, no. 12, pp. 787–791, Dec. 2011.

[29] D. Kwon and G.A. Rincón-Mora, "A 2-um BiCMOS Rectifier-Free AC-DC Piezoelectric Energy Harvester-Charger IC," *IEEE Trans. on Biomedical Circuits Syst.*, vol. 4, no. 6, pp.400–409, Dec. 2010.

[30] D. Kwon and G.A. Rincón-Mora, "A Single-inductor ac-dc piezoelectric energy-harvester/battery-charger IC converting +-(0.35 to 1.2V) to (2.7 to 4.5V)," in *IEEE Int. Solid-State Circuits Conf.*, pp. 494–495, Feb. 2010.

[31] P. Gasnier, J. Willemin, S. Boisseau, G. Despesse, C. Condemine, G. Gouvernet, and J.J. Chaillout, "An Autonomous Piezoelectric Energy Harvesting IC Based on a Synchronous Multi-Shot Technique," *IEEE Journal of Solid-State Circuits*, vol. 49, no. 7, pp. 1561–1570, July 2014.

[32] E.E. Aktakka and K. Najafi, "A Micro Inertial Energy Harvesting Platform With Self-Supplied Power Management Circuit for Autonomous Wireless Sensor Nodes," *IEEE Journal Solid-State Circuits*, vol. 49, no. 9, pp. 2017–2029, Sep. 2014.

[33] M. Dini, A. Romani, M. Filippi, and M. Tartagni, "A Nanopower Synchronous Charge Extractor IC for Low-Voltage Piezoelectric Energy Harvesting With Residual Charge Inversion," *IEEE Trans. on Power Electronics*, vol. 31, no. 2, pp. 1263–1274, Feb. 2016.

[34] I.M. Darmayuda, Y. Gao, M.T. Tan, S.J. Cheng, Y. Zheng, M. Je, and C.H. Heng, "A Self-Powered Power Conditioning IC for Piezoelectric Energy Harvesting from Short-Duration Vibrations", *IEEE Trans. Circuits Syst. II, Exp. Briefs*, vol. 59, no. 9, pp. 578–582, Sep. 2012.

[35] Y. Rao and D.P. Arnold, "Input-Powered Energy Harvesting Interface Circuits with Zero Standby Power," *IEEE Trans. on Power Electronics*, vol. 26, no. 12, pp. 3524–3533, Dec. 2011.

[36] G.K. Ottman and H.F. Hofmann, "Optimized Piezoelectric Energy Harvesting Circuit Using Step-Down Converter in Discontinuous Conduction Mode," *IEEE Trans. on Power Electronics*, vol. 18, no. 2, pp. 696–703, Mar. 2003.

[37] D. Kwon, G.A. Rincón-Mora, and E.O. Torres, "Harvesting Ambient Kinetic Energy with Switched-Inductor Converters," *IEEE Trans. on Circuits and Systems I*, vol. 58, no. 7, pp. 1551–1560, July 2011.

[38] D. Kwon and G.A. Rincón-Mora, "A single-inductor 0.35-um CMOS energy-investing piezoelectric harvester," *IEEE Int'l Solid-State Circuits Conf.*, Feb. 2013.
[39] J. Dicken, P.D. Mitcheson, I. Stoianov, and E.M. Yeatman, “Increased power output from piezoelectric energy harvesters by pre-biasing,” in *Proc. PowerMEMS*, pp. 75–78, Dec. 2009.
[40] J. Dicken, P.D. Mitcheson, I. Stoianov, and E.M. Yearman, “Power-Extraction Circuits for Piezoelectric Energy Harvesters in Miniature and Low-Power Applications,” *IEEE Trans. on Power Electronics*, vol. 27, no. 11, pp. 4514–4529, Nov. 2012.
[41] E. Lefeuvre, A. Badel, C. Richard, L. Petit, and D. Guyomar, “A Comparison Between Several Vibration-Powered piezoelectric Generators for Standalone Systems”, *Sensors Actuators A Physical*, vol. 126, no. 2, pp. 405–416, Feb. 2006.
[42] J. Dicken, P.D. Mitcheson, A. Elliott, and E.M. Yeatman, “Single-Supply Pre-Biasing Circuit for Low-Amplitute Energy Harvesting Applications”, in *Proc. Power MEMS*, pp. 46–49, Nov. 2009.
[43] D. Kwon and G.A. Rincón-Mora, “A single-Inductor 0.35 um CMOS Energy-Investing Piezoelectric Harvester,” *IEEE J. Solid-State Circuits*, vol. 49, no. 10, Oct. 2014.
[44] D. Guyomar, A. Dadel, E. Lefeuvre, and C. Richard, “Toward Energy Harvesting Using Active Materials and Conversion Improvement by Nonlinear Processing”, *IEEE Trans. Ultrason. Ferroelectr. Freq. Control*, vol. 52, no. 3, pp. 584–595, Apr. 2005.
[45] C.S. Lee, H.Y. Choi, Y.S. Kim, and N.S. Kim “A Low-Power CMOS DC-DC Buck Converter with On-Chip Stacked Spiral Inductor,” *Microelectronics Int.*, vol. 28, no. 2, pp. 38–43, Feb. 2011.

Gabriel A. Rincón-Mora (SM'90, GM'93, M'97, SM'01, F'11) worked for Texas Instruments in 1994–2003, was an Adjunct Professor at Georgia Tech in 1999–2001, and has been a Professor at Georgia Tech since 2001 and a Visiting Professor at National Cheng Kung University in Taiwan since 2011. He is a Fellow of the IET and his scholarly products include 9 books, 4 book chapters, 38 patents issued, over 160 publications, over 26 commercial power-chip designs, and over 95 invited talks. Awards include the National Hispanic in Technology Award from the Society of Professional Hispanic Engineers, the Charles E. Perry Visionary Award from Florida International University, a Commendation Certificate from the Lieutenant Governor of California, the IEEE Service Award from IEEE CASS, the Orgullo Hispano and the Hispanic Heritage awards from Robins Air Force Base, and two "Thank a Teacher" certificates from Georgia Tech. Georgia Tech inducted him into the Council of Outstanding Young Engineering Alumni in 2000 and Hispanic Business magazine named him one of "The 100 Most Influential Hispanics" in 2000.

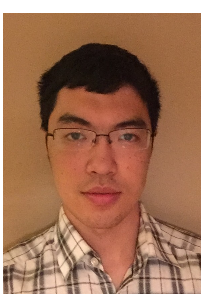

Siyu Yang (GM'14) received the B.S. degree in Microelectronics from Tsinghua University, China in 2013. He is currently pursuing the Ph.D degree in electrical engineering from Georgia Institute of Techology, Atlanta. His research interests include piezoelectric energy harvesting circuit, low-power analog IC design, and power integrated circuits (ICs).